Enhanced macromolecular substance extravasation through the blood-brain barrier via acoustic bubble-cell interactions

Jifan Chen, Jean-Michel Escoffre, Oliver Romito, Tarik Iazourene, Antoine Presset, Marie Roy, Marie Potier Cartereau, Christophe Vandier, Yahua Wang, Guowei Wang, et al.

Ultrasonics Sonochemistry 103 (2024) 106768

Contents lists available at ScienceDirect

Ultrasonics Sonochemistry

journal homepage: www.elsevier.com/locate/ultson

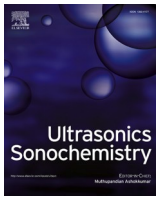

Enhanced macromolecular substance extravasation through the blood-brain barrier via acoustic bubble-cell interactions

Jifan Chen [a,b], Jean-Michel Escoffre [b], Oliver Romito [c], Tarik Iazourene [b], Antoine Presset [b], Marie Roy [b], Marie Potier Cartereau [c], Christophe Vandier [c], Yahua Wang [b], Guowei Wang [a], Pintong Huang [a,d,1,*], Ayache Bouakaz [b,1,*]

[a] Department of Ultrasound in Medicine, The Second Affiliated Hospital of Zhejiang University, School of Medicine, Zhejiang University, Zhejiang, China
[b] Inserm UMR 1253, iBrain, Université de Tours, Inserm, Tours, France
[c] Inserm UMR 1069 Nutrition, Croissance et Cancer (N2C), Faculté de Médecine, Université de Tours, F-37032, France
[d] Research Center for Life Science and Human Health, Binjiang Institute of Zhejiang University, Hangzhou 310053, China

ARTICLE INFO

Keywords:
Ultrasound
Microbubbles
Bubble-cell mechanical interaction
Blood-brain barrier
Macromolecular substance
Transcytosis
Drug delivery
In-vitro

ABSTRACT

The blood–brain barrier (BBB) maintains brain homeostasis, regulates influx and efflux transport, and provides protection to the brain tissue. Ultrasound (US) and microbubble (MB)-mediated blood–brain barrier opening is an effective and safe technique for drug delivery *in-vitro* and *in-vivo*. However, the exact mechanism underlying this technique is still not fully elucidated. The aim of the study is to explore the contribution of transcytosis in the BBB transient opening using an in-vitro model of BBB. Utilizing a diverse set of techniques, including Ca^{2+} imaging, electron microscopy, and electrophysiological recordings, our results showed that the combined use of US and MBs triggers membrane deformation within the endothelial cell membrane, a phenomenon primarily observed in the US + MBs group. This deformation facilitates the vesicles transportation of 500 kDa fluorescent Dextran via dynamin-/caveolae-/clathrin- mediated transcytosis pathway. Simultaneously, we observed increase of cytosolic Ca^{2+} concentration, which is related with increased permeability of the 500 kDa fluorescent Dextran *in-vitro*. This was found to be associated with the Ca^{2+}-protein kinase C (PKC) signaling pathway. The insights provided by the acoustically-mediated interaction between the microbubbles and the cells delineate potential mechanisms for macromolecular substance permeability.

1. Introduction

In the brain and spinal cord of mammals, including humans, the permeability of blood–brain barrier (BBB) is controlled by tight junctions between endothelial cells, which restrict the diffusion of pathogenic microorganisms and large hydrophilic molecules (>400 Da) from the bloodstream into the brain parenchyma [1]. The primary functions of BBB are maintaining brain homeostasis, regulating influx and efflux transport, and protecting brain tissue from harm [2]. Besides, endothelial cells of CNS exhibit low levels of vesicle trafficking, which is generally assumed to limit transcellular transport [3]. These physiological phenomenon prevent therapeutic molecules from passing through the capillary and diffusing freely and deeply into brain tissue or lesions. Several drug delivery methods including direct brain infusion [4], convection-enhanced delivery [5], and biophysical methods have been developed in order to enhance the intracerebral bioavailability of therapeutic molecules [6,7]. The macromolecules such as proteins, antibodies, and nanomedicines can be delivered into brain through the transcytosis effect by using specific endothelial receptors or membrane structures [8]. Unfortunately, the expression of the major facilitator superfamily domain containing protein 2a (Mfsd2a) in the human brain endothelial cells has been identified as a negative regulation factor for transcytosis of BBB. Specifically, when Mfsd2a is overexpressed, it significantly inhibits the process of transcytosis within the endothelial cells of the central nervous system (CNS). Compared with wide type mice, the traffic vesicles in the endothelial cells of Mfsd2a knock-out mice exhibited a significant elevation [3,9,10]. The key vesicular structures involved in transcytosis such as clathrin-coated pits and

* Corresponding authors at: Department of Ultrasound in Medicine, The Second Affiliated Hospital of Zhejiang University, School of Medicine, Zhejiang University, Zhejiang, China (P. Huang).
E-mail addresses: huangpintong@zju.edu.cn (P. Huang), ayache.bouakaz@univ-tours.fr (A. Bouakaz).
[1] These authors contributed equally to this work.

https://doi.org/10.1016/j.ultsonch.2024.106768
Received 28 July 2023; Received in revised form 1 January 2024; Accepted 14 January 2024
Available online 17 January 2024

caveolae, which are responsible for the internalization of macromolecules or nanoparticles and their transport across the endothelial cell from one side to the other side [11]. These findings emphasize the critical role of Mfsd2a expression in modulating the intricate mechanisms underlying transcytosis within the BBB.

As one of the promising approaches, the BBB opening (BBBO) using microbubble-assisted ultrasound (MB-assisted US) has been investigated in *in-vitro* studies [12], preclinical studies [13], and being currently evaluated in a few clinical trials [14]. By employing low intensity pulsed US, it is possible to induce MBs oscillations characterized by expansions and contractions. These oscillations result in a transient opening of endothelial tight junctions [15]. In addition, it has been reported that in-vivo, there is an increase in caveolae-mediated transcytosis following the application of US + MBs for larger cargo (>500 kDa). But the phenomena were not found in smaller cargo (3 or 70 kDa). These results shed light on an additional mechanism of acoustically-mediated macromolecule transport [16,17]. It has been also reported that the MBs-cell mechanical interactions stimulate the formation of transient pits, ranging from a few nanometers to 150 nm *in-vitro* [18]. Furthermore, in an *in-vivo* scenario, it has been reported that the group treated with US + MBs exhibited increased number of pinocytotic vesicles and higher levels of caveolin-1 expression compared to the groups not exposed to US [17]. Moreover, the influx of Ca^{2+} into the cytosol during the acoustically mediated pore formation might enhance the cellular physiological responses, including calcium-related signal pathway activation, elevated endocytosis and increased vascular permeability [19,20]. Additionally, the generation of reactive oxygen species (ROS) resulting from cavitation-induced sonochemistry may contribute to the permeabilization of the cell membrane using MB-assisted US. This can occur through the oxidation of lipid membrane [21,22].

Until now, the biophysical mechanism behind the transcytosis induced by the combination of US + MBs remains unclear. In the current research study, our hypothesis explores the potential role of mechanical interactions between microbubbles and cells, facilitated by the application of ultrasound in promoting the enhanced extravasation of large molecules across the BBB. To investigate this hypothesis, we utilize an *in vitro* model of the BBB and employ various techniques such as calcium imaging, electron microscopy, and electrophysiological recordings. Through these experimental approaches, we aim to unravel the mechanisms underlying the increased transcytosis observed during the use of US + MBs and gain valuable insights into this phenomenon.

2. Materials and methods

2.1. Chemicals

Fluorescent dextrans of 3 kDa (D3306) and 500 kDa (D7136) were purchased from Thermo Fisher Scientific Inc (USA).

2.2. Microbubbles

Vevo MicroMarker™ contrast agents were purchased from Fujifilm-VisualSonics (Toronto, Canada). These agents were prepared according to the manufacturer's instructions. The final concentration of microbubbles (MBs) was 2×10^9 MBs/mL.

2.3. Cell culture

Human microvascular brain endothelial cell line (hCMEC/D3; SCC066) were purchased from Merck Millipore (Fontenay sous Bois, France). These cells were cultured as a monolayer in EndoGRO-MV medium (Merck Millipore).

2.4. Acoustic equipment

Ultrasound waves were generated using a single-element transducer (Sofranel, Sartrouville, France) with a center frequency of 1 MHz. The transducer had a diameter of 15 mm and was naturally focused at 27 mm. It was driven by an arbitrary waveform generator (33250A, Agilent Scientific Instruments, USA), then amplified by a 500 W power amplifier (AAP-500–0.2–6-D; ADECE, Vallauris, France). The peak negative pressure of the acoustic wave was measured in a separate setup using a calibrated hydrophone (HGL-0200, ONDA Corporation) at the natural focal distance of the transducer.

2.5. Sonoporation device

A custom-made device for ultrasound application in viability and transcytosis experiment has been designed by AP (Figure S1). A Transwell® insert (Corning, Shanghai, China) of hCMEC/D3 cells was inverted and fixed in the device. The transducer was placed at the bottom of the device at a 27 mm distance from the insert surface. The MBs were injected into the device and they floated in contact to the cell monolayer. An acoustic absorber was placed on the top of the device in order to avoid acoustic reflections. Besides, in endocytosis, exocytosis, calcium imaging, and electron microscope experiment, the other custom-made device designed by JME was used as previously reported [18].

2.6. In-vitro BBB permeability

A hCMEC/D3 monolayer was cultured in the apical compartment of the Transwell® insert. The transendothelial electrical resistance (TEERs, EVOM2, Sarasota, USA) of the *in-vitro* BBB reached 50 Ω/cm^2, demonstrating the barrier integrity compared to the insert without endothelial cells. To investigate the effect of the MB, a MB:cell ratio of 50:1 was used. The *in-vitro* BBB was then subjected to 1 MHz sinusoidal US waves, consisting of pulses of 50 cycles and repeated every 1 ms and at a peak negative pressure $\lesssim$ 0.5 MPa. The total exposure time to the US waves was 2 min. The insert was immediately placed in suitable culture plate. Besides, fluorescent dextrans (3 kDa or 500 kDa) were immediately added into the upper chamber. A volume of 1.5 mL of phosphate buffered saline (PBS; Thermo Fisher, USA) solution was added into the bottom chamber. Then, this chamber was sampled at 0 and 1 h. The difference between pre- and post-US + MBs treatments in TEER values and fluorescent intensities were measured to monitor the BBB permeability. The positive control group was defined as experiment group without adherent cell.

2.7. Cell viability assessment

The influence of peak negative pressures (0, 0.1, 0.3, 0.5, 0.7 MPa) on the viability of BBB was assessed using a 3-(4,5-dimethylthiazol-2-yl)-2,5-diphenyltetrazolium bromide colorimetric assay (MTT; ThermoFisher Scientific, USA) assay. After incubating with MTT reagent for 1 h, 10 μL sample was added in transparent 96-well plate per group. Afterwards, the optical density (OD) was measured at 570 nm.

2.8. Endocytosis and transcytosis analysis for macromolecules

2.8.1. Endocytosis analysis

To investigate the endocytosis process, the adherent *in-vitro* BBB were incubated with 500 kDa fluorescent Dextran and treated with US + MBs synchronously. Then, the samples of fluorescent suspensions were collected at different incubating times and measured using a fluorescent plate reader (FLUOstar OPTIMA, BMG Lab tech, Germany). Besides, the adherent cells digested by trypsin were collected at 2 h post-treatment and the cell suspension was measured by flow cytometer (FCM) (CytoFLEX, Beckman Coulter, Inc., USA).

2.8.2. Transcytosis analysis

To investigate the relationship between US + MBs and the transcytosis pathway, Dynasore hydrate (Dy, 50 μM, an inhibitor of dynamin-

mediated pathway), Methyl-β-cyclodextrin (Mβc, 800 μM, an inhibitor of Caveolae-mediated pathway), and Pitstop2 (PP2, 20 μM, an inhibitor of clathrin-mediated pathway) were pre-incubated with the monolayer for 1 h separately. Then, 500 kDa fluorescent Dextran was added into the upper chamber after US + MBs treatment. The PBS solution in the bottom chamber was sampled at 0 and 2 h and the fluorescent intensity was measured using fluorescent plate reader.

2.9. Cell electrophysiology

2.9.1. Protocol

The patch-clamp technique in the whole-cell configuration was used to monitor the modification of electrical plasma membrane properties induced by US + MBs [23]. A custom device was designed by JC to perform patch-clamp experiments. An inverted microscope (Eclipse® TE300, Nikon, Champigny sur Marne, France) was used on an anti-vibration table (TMC, Peabody, MA). hCMEC/D3 cells were cultured on 35-mm culture dishes (CELLSTAR® Greiner bio-one, Germany) at 1500 cells/cm^2. Two or three days later, the cell monolayer was washed and the medium was replaced with standard bath solution (SBS) (in mM): 130 NaCl, 5 KCl, 8 D-glucose, 10 HEPES, 1.2 $MgCl_2$, and 1.5 $CaCl_2$ (set to pH 7.4 with NaOH) before the patch-clamp experiments. Patch pipettes were prepared from nonheparinized hematocrit tubes (Vitrex, Paris, France) to a resistance of 4–10 MΩ using a puller (Sutter Instrument Co., Novato, CA). The pipette solution was prepared as below: (in mM): 130 KCl, 10 NaCl, 0.5 $MgCl_2$, 5 Mg-ATP, 0.5 EGTA, 10 HEPES, and 0.4 GTPTris (set to pH 7.2 with KOH). At room temperature, whole-cell membrane potentials were recorded under a current-clamp mode with no current injected (I = 0) using an Axopatch® 200B patch clamp amplifier (Axon Instrument, Burlingame, CA). Analog signals were filtered at 5 kHz using a five-pole low pass Bessel filter and sampled at 10 kHz using a 1322A Digidata converter (Axon Instrument, Burlingame, CA). PClamp® software (v.9.2, Axon Instrument, Burlingame, CA) was used for the current-clamp, acquisition, and analysis of results.

2.9.2. Patch-clamp data post-processing

In order to remove the systematic noise originating from the transducer and power amplifier, a low pass filter was implemented using the fast Fourier transform (FFT) using Matlab software (Mathworks, USA). Then, both the systematic noise (resulting from the transducer and power amplifier) and random noise were filtered out, enabling the extraction of the electrical signal generated by acoustically stimulated cells.

2.10. Cytosolic Ca^{2+} and Ca^{2+} related pathway

Fluo-4-AM (HY-101896; MedChemExpress, USA) was used to detect the relative cytosolic Ca^{2+} concentration change. The working concentration and incubating time of Fluo-4-AM were 1 mM and 20 min respectively. The cell was washed thrice by PBS before US + MBs. For fluorescent images, the cells were fixed using 4 % paraformaldehyde (PFA) immediately after exposing to US + MB. To investigate the relationship between Ca^{2+} related pathways and the transcytosis, Rottlerin (20 μM, an inhibitor of Protein kinase C pathway, PKC) and KN-93 (100 nM, an inhibitor of Ca^{2+}/calmodulin-dependent protein kinase II, CaMKII) were pre-incubated with the cell monolayer for 1 h in the transcytosis experiment separately.

2.11. Electron microscope experiment

The effects of MB-assisted US on the cell ultrastructure and specifically, on plasma membrane were investigated using scanning electron microscopy (SEM). Briefly, hCMEC/D3 cells were cultured on coverslip. After US + MBs, they were fixed with a solution of 4 % PFA and 1 % glutaraldehyde in 0.1 M phosphate buffer (pH 7.2) at 4 ℃ for 48 h. SEM specimens were dehydrated in a graded series of ethanolic solution (50 % – 100 %) and critical points dried in liquid carbon dioxide. The coverslips were attached to sample stubs and sputtered coating with platinum (5 nm). SEM of our samples were performed using a LEO DSM 982 SEM (Zeiss, Germany).

2.12. Statistical analysis

The GraphPad Prism 8.0 software was used in this study. Data were presented as mean ± standard deviations. One-way ANOVA and Tukey correction were used to test the difference's statistical significance among groups. Statistical significance was defined as $p < 0.05$ (NS, non-significance, *$p < 0.05$, **$p < 0.01$ and ***$p < 0.001$).

3. Results

3.1. The viability analysis

The influence of peak negative pressures (from 0 to 0.7 MPa) on BBB viability was assessed using MTT colorimetric assay after US + MBs exposure. No statistically significant difference in BBB viability was observed for the PNPs of 0, 0.1, 0.3 and 0.5 MPa compared to the control condition. However, the exposure of BBB to a PNP of 0.7 MPa induced a significant decrease of the BBB viability in comparison to the control condition (Fig. 1A).

3.2. The role of extracellular Ca^{2+} ions on the acoustically-mediated opening of BBB

To investigate the role of Ca^{2+} on the US + MBs-mediated opening of the BBB *in-vitro*, various experimental groups were examined for changes in the TEERs and the transport of fluorescent dextrans (3 kDa and 500 kDa) in the presence or absence of Ca^{2+}. When Ca^{2+} were present, the application of US + MBs at 0.5 MPa resulted in a significant decrease in TEERs compared to when Ca^{2+} were absent (Fig. 1B). In addition, exposure of the BBB to US + MBs led to a much higher fluorescent intensity at the bottom of the chamber for both dextran molecular weights when Ca^{2+} ions were present (Fig. 1C and D), confirming the findings of the TEER experiments. Also, in the absence of Ca^{2+}, the US + MBs treatment induced a significant increase in fluorescent intensity at the bottom of the chamber for both molecular weights of fluorescent dextrans compared to control groups.

3.3. Effects of US + MBs on cellular electrophysiology and cytosol Ca^{2+} concentration

During the patch clamp measurement, the hCMEC/D3 cellular monolayer was exposed to US + MBs. Membrane potential were acquired using the whole-cell configuration approach in current clamp mode, followed by post-processing to remove the background noise. As shown in Fig. 2A, the hyperpolarization during US + MBs was recorded, occurred during the exposure to US + MBs followed by a return to baseline once the US was discontinued.

In addition, the impact of US + MBs on the cytosolic Ca^{2+} concentration in hCMEC/D3 monolayers was assessed through Ca^{2+} fluorescence imaging (Fig. 2B and 2C). The results indicate that the US + MBs treatment engendered a higher Ca^{2+} fluorescent intensity than the control conditions. In addition, the exposure of cell monolayer to US + MBs in the presence of ascorbic acid (AA, ROS scavenger) induced a lower Ca^{2+} fluorescent intensity than that of cell monolayer treated with US + MBs alone. These findings reveal that the combined effect of US + MBs results in alterations in the cell membrane potentials and in the cytosolic Ca^{2+} concentration via both mechanical and sonochemical effects. The increased cytosolic Ca^{2+} caused by US + MBs can be explained by mechanical interplay between oscillating MBs and the cell's plasma membrane, directly affecting the membrane integrity by the pushing and pulling of the plasma membrane. Besides, the

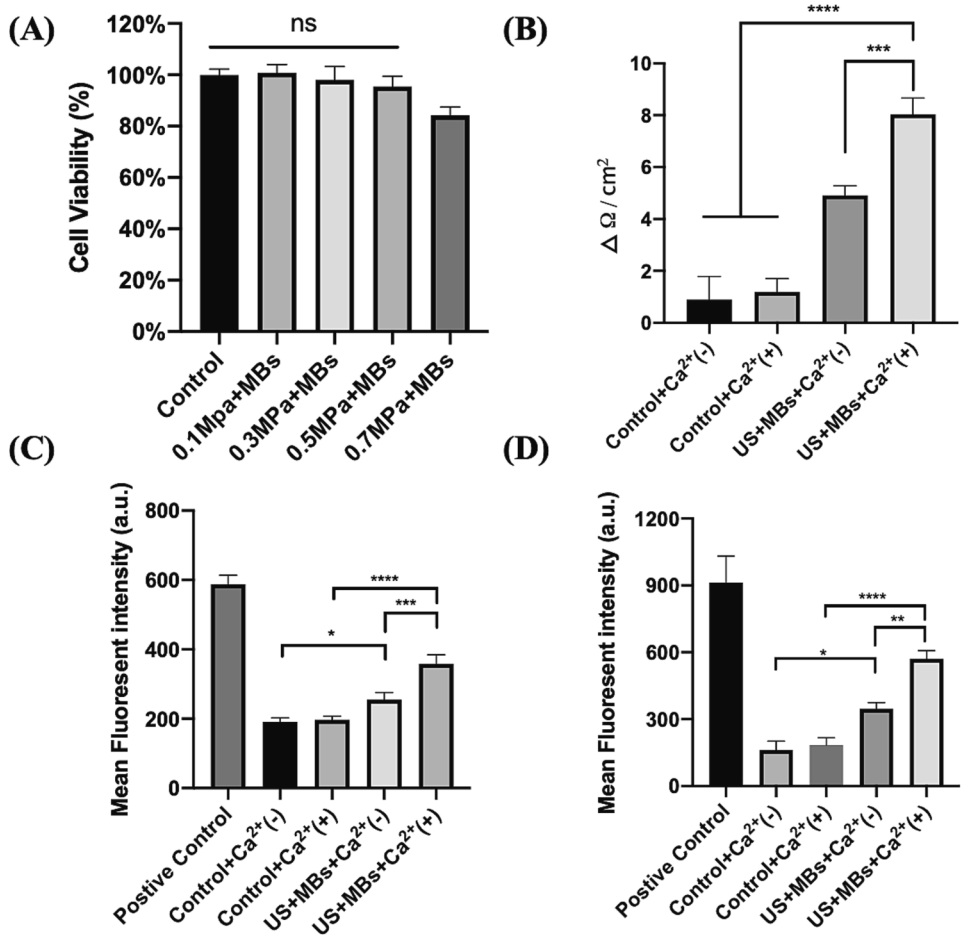

Fig. 1. The role of extracellular Ca^{2+} on the acoustically-mediated opening of BBB *in-vitro* (A) cell viability experiment (B) TEERs value (C) Mean 3 kDa dextran fluorescence intensity at the bottom of the chamber (D) Mean 500 kDa dextran fluorescent intensity at the bottom of the chamber; Positive Control: group without hCMEC/D3 cell (3 independent replicates).

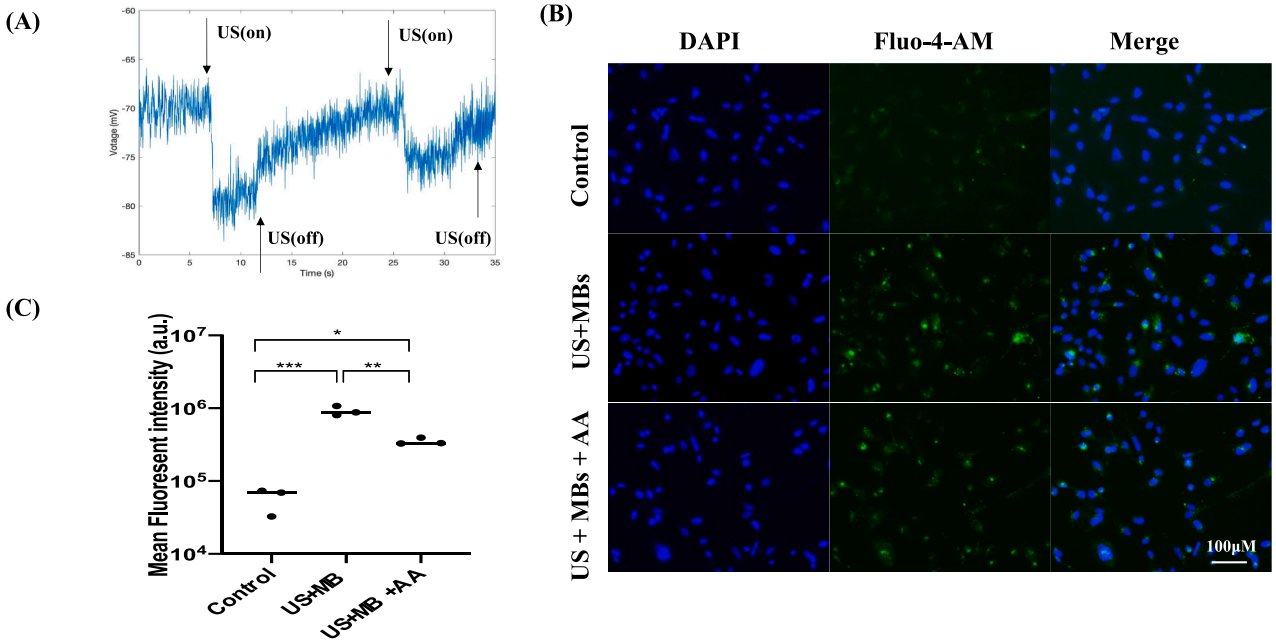

Fig. 2. US + MBs mediated cellular electrophysiology change and Ca^{2+} influx (A) Membrane potential during US + MBs by real-time patch clamp recording (5 independent replicates); (B) Cytosolic calcium fluorescence imaging; (C) Mean fluorescence intensity of Cytosolic calcium ion in the different groups (3 independent replicates).

sonochemical reactions triggered by cavitation microbubbles can produce reactive oxygen species (ROS). These ROS can induce excessive oxidation of the plasma membrane, and hence compromising its structural integrity.

3.4. Enhanced transport of 500 kDa fluorescent dextran across the BBB by US + MBs

The effects of MB-assisted US on the transport of 500 kDa fluorescent dextran through a hCMEC/D3 barrier were investigated using scanning electron microscopy (SEM). SEM images revealed the presence of 0.5–1 μm pits on the surface of cell membrane of hCMEC/D3 barrier exposed to US + MBs. This observation provides direct evidence of the direct interaction between the membrane and the MBs (Fig. 3A). Concurrently, an increasing number of smaller 50–100 nm pits was also noted, indicating an increase in membrane permeability. The transcellular transport of 500 kDa fluorescent dextran was investigated by introducing a transcytosis inhibitor, Dynasore hydrate (Dyn). Prior to exposure to US + MB and fluorescent dextran, the hCMEC/D3 barrier was preconditioned with Dyn for 1 h. Post-treatment, the fluorescence intensity at the bottom of the chamber was significantly decreased compared to the hCMEC/D3 barrier treated solely with US + MBs (Fig. 3B).

In addition, to investigate the role of acoustically generated ROS, the hCMEC/D3 barrier was incubated with AA for ROS scavenging purposes. There was no significant difference in fluorescence intensity observed at the bottom chamber of hCMEC/D3 barriers treated with US + MBs in the presence or in absence of AA (Fig. 3C). However, when the hCMEC/D3 barrier was treated either with MBs or with H_2O_2 or a combination of H_2O_2 and AA, the fluorescent intensity was lower compared to the group exposed to US + MBs with or without AA. These findings demonstrate the significance of the mechanical interaction between MBs and plasma membrane of hCMEC/D3 cells, surpassing the impact of ROS in facilitating this transcellular process.

3.5. Internalization mechanisms of 500 kDa Dextran: Involvement of Ca^{2+} and Caveolae/Clathrin-mediated endocytosis

In order to elucidate the involvement of Ca^{2+} in the intracellular transports of 500 kDa dextran, we conducted an experiment to determine the role of Ca^{2+} in the process of endocytosis. After incubating with 500 kDa Dextran and exposing to US + MBs, we sampled the fluorescence intensity of cell-free supernatant, representing the residual 500 kDa dextran, at different time points. In addition, we used flow cytometry to measure the cellular fluorescence intensity, which refers to the cellular endocytosis of 500 kDa dextran, in different control and experimental groups after a 2-hour incubation period.

As shown in Fig. 4A, the US + MBs + Ca^{2+} group exhibited significant decrease in fluorescence intensity compared to the control groups. Besides, the flow cytometry analysis showed that the 500 kDa dextran-intake positive cell rate in US + MBs + Ca^{2+} group is higher than in the other groups (Fig. 4B). In addition, the intracellular internalization of 500 kDa fluorescent dextran was found to be inhibited by Dy, Mβc, and PP2, thus demonstrating the vital role of the caveolae- or clathrin-mediated pathways in the endocytosis of 500 kDa fluorescent dextran (Fig. 4C).

3.6. Involvement of Caveolae-/Clathrin-mediated and Ca2 + -Dependent pathways in transcytosis induced by US + MBs

When the hCMEC/D3 barrier is incubated with specific transcytosis inhibitors (Mβc and PP2), the fluorescence intensity at the bottom chamber decreased significantly indicating the involvement of both the caveolae- and clathrin-mediated transcytosis pathways in the trans-endothelial transport of 500 kDa dextran (Fig. 5A). To further investigate the calcium-related pathway, we conducted pretreatement experiment using Rotterin and KN93 in the transcytosis experiment respectively. The fluorescence intensity at the bottom chamber in the US + MBs + Rotterin group was partially decreased. However, no obvious decrease was observed in the US + MBs + KN93 group (Fig. 5B).

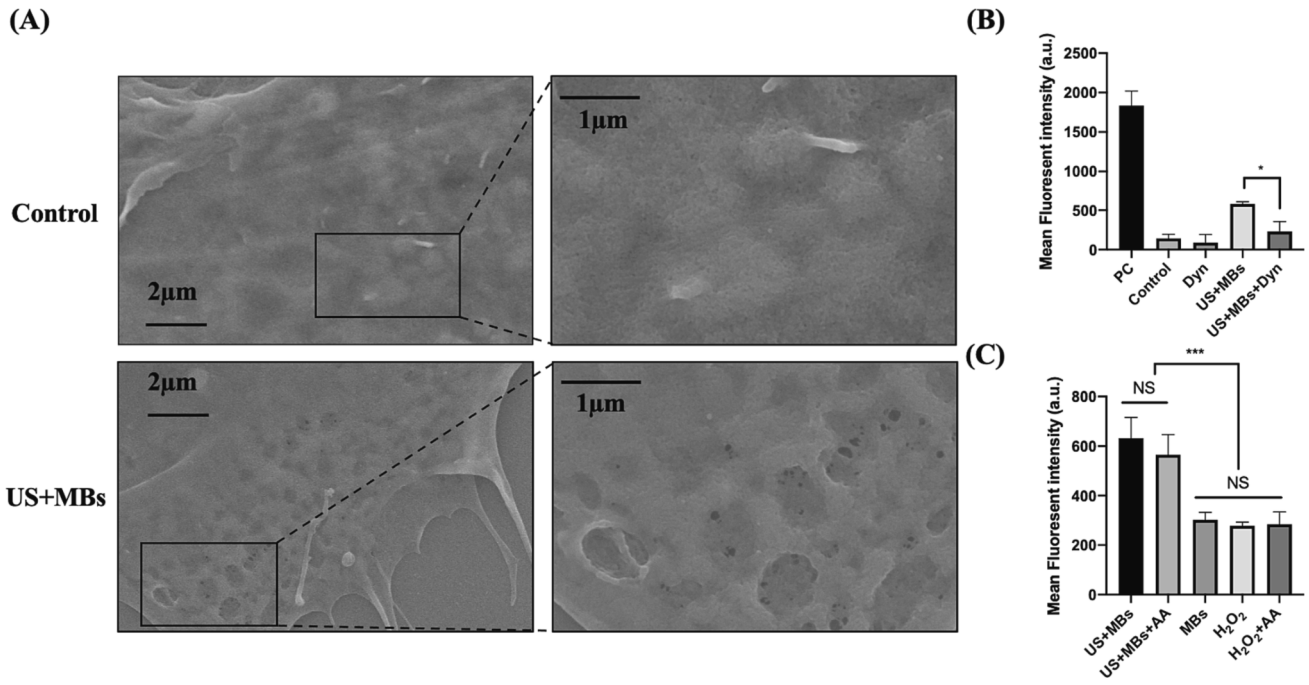

Fig. 3. The US + MBs mediated leakage of 500 kDa Dextran through the transcellular pathway (A)The non-US + MBs treatment group (The top figure), The US + MBs treatment group (The bottom figure); (B)Mean fluorescence intensity in bottom chamber among different groups; (C) Mean fluorescence intensity in bottom chamber among different groups (3 independent replicates).

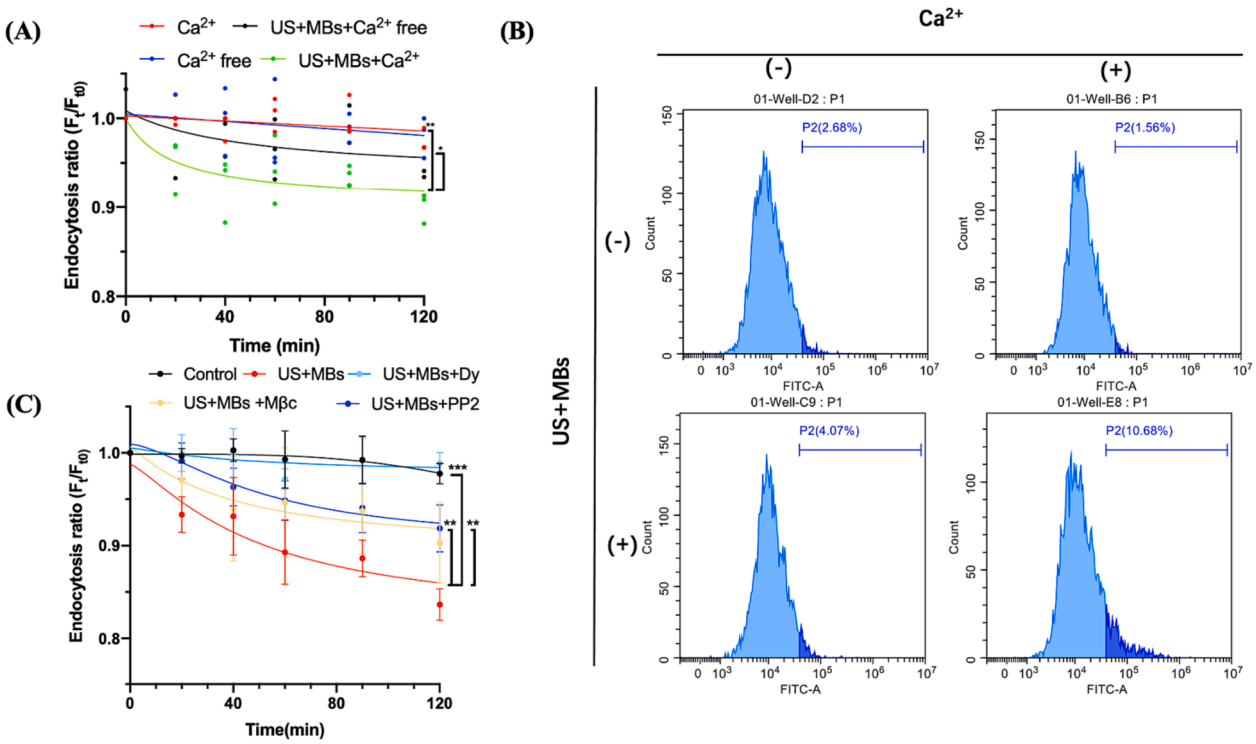

Fig. 4. Ca^{2+} assisted and Caveolae-/Clathrin-mediated Endocytosis of 500 kDa Dextran (A) Fluorescence intensity in suspensions after different time point with/without calcium ions. (B) The cellular fluorescence intake after different time point with/without calcium ions. (C) Fluorescence intensity in suspensions after different time point with different inhibitors (3 independent replicates).

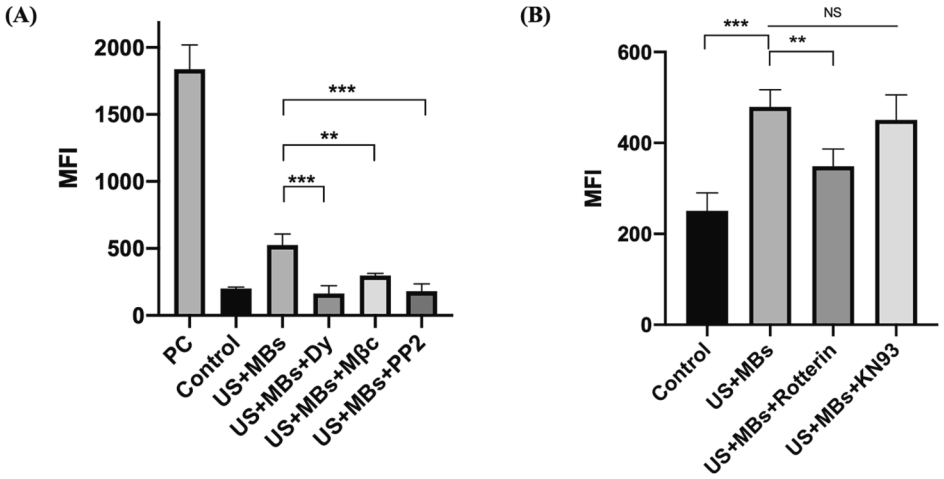

Fig. 5. Caveolae-/Clathrin-mediated and a Ca^{2+}-dependent pathway participate in the US + MBs induced transcytosis (A)The mean fluorescence intensity in the bottom chamber with different transcytosis inhibitors; (B) The mean fluorescence intensity in the bottom chamber with different calcium-related pathway inhibitors (3 independent replicates).

4. Discussion

This study investigates the mechanical interactions between bubbles and cells. Our experimental results demonstrate that the deformation of the cell membrane plays a crucial role in facilitating the necessary bubble-cell interactions necessary for inducing transendothelial transport of 500 kDa fluorescent dextran in an in-vitro BBB model using hCMEC/D3. Additionally, the formation of the membrane pores through acoustic exposure leads to increase the membrane hyperpolarization, elevate cytosolic Ca^{2+} thus accelerating the transcytosis of 500 kDa dextran. According to our hypothesis, the mechanical interaction between cell membrane and oscillating MBs is necessary to trigger this transcytosis process. The formation of pits on the surface of cellular membrane, induced by the combination of US + MBs, may enhance the transcytosis effect of 500 kDa dextran. Meanwhile, the increased cytosolic Ca^{2+} concentration accelerates the acoustically mediated transendothelial transport of this dextran through calcium-dependent pathways, including the Ca^{2+}-PKC pathway.

In addition, we have observed that acoustically generated ROS can take part in the process of increased cytosolic Ca^{2+} concentration. This phenomenon is consistent with the previous findings that have demonstrated the involvement of ROS in the cell sonoporation [22]. Moreover, previous studies reported that ROS promote caveolae-mediated transcytosis via Rac1 signaling and c-Src-dependent

caveolin-1 phosphorylation in human brain endothelial cells [24]. This could potentially be a putative explanation in the acoustically mediated caveolae-mediated transcytosis. However, based on our current understanding, these ROS are mainly generated from MB cavitation, which might have limited diffusion into cytoplasm because of the short diffusion distance. So, we speculate that the acoustically mediated ROS might mainly contribute to the lipid over-oxidation, which weakens the cellular membrane, facilitating the formation of membrane pores, promoting Ca^{2+} influx, increasing the cytosolic Ca^{2+} concentration and aiding transcytosis indirectly.

Besides, it has been reported that the acoustically-mediated mechanical forces can induce Ca^{2+} influx through the formation of membrane pores [19] and the activation of mechanosensitive channels (MSCs) [25]. However, in our study, we did not observe a significant difference in the transcytosis experiment when using several inhibitors of MSCs. This could potentially be attributed to the varying expression levels of MSC proteins in endothelial cell lines, including within the same cell line (hCMEC/D3) [26,27]. In a previous study, we reported the acoustically-mediated formation of membrane pores [18]. Interestingly, even in the presence of ROS scavenger (AA), the fluorescent signal of Ca^{2+} remained higher than in the control group. This suggests that both ROS generation and mechanical interaction between cells and MBs contribute to an increased ratio of pore formation and Ca^{2+} influx.

Ca^{2+} have been identified as a key factor in both endocytosis [19,28] and exocytosis [29,30] processes. The transcytosis process, including clathrin- and caveolae-mediated transcytosis, facilitates the transport of macromolecules (nanodrugs, proteins, nanoparticles, *etc.*) [31,32] across endothelial cells. The transient membrane pores induced by US + MBs results in membrane hyperpolarization. This hyperpolarization can be attributed to an increase in outward potassium current amplitudes, which subsequently increases the driving force for calcium in the cytosol thus increasing cytosolic calcium concentration [23]. The cytosolic Ca^{2+} activates the Ca^{2+}-related proteins, such as PKC, initiating downstream phosphorylation/dephosphorylation events and then will facilitate special biological functions, including endocytosis [33].

Dynamin is an essential component of both clathrin-dependent and caveolar-dependent endocytosis, plays a role in the invagination of cell plasma membrane to form a budding vesicle [34,35]. Following the application of US + MBs, membrane pits appear as a result of the mechanical force exerted by the oscillating microbubbles, which seem to be the initial step of transcytosis. Furthermore, our data demonstrate that both clathrin-dependent and caveolar-dependent pathways are involved in the acoustically mediated transcytosis.

Our study does face however certain limitations. Our monocultured endothelial cell model, while informative, cannot fully replicate the multifaceted BBB. Disparities in cellular electrophysiology between our model and an intact endothelial layer are also acknowledged. Furthermore, we pinpoint the investigation of mechanical sensitivity channels on the endothelial membrane as critical to deepening our understanding of endothelial function, proposing this as a directive for future research work.

To summarize, when combined with US stimulation, microbubbles interact the cell plasma membrane of hCMEC/D3 monolayer, causing a direct membrane deformation. This interaction generates both mechanical and sonochemical effects. In this process, pit formation occurs and seems to be the crucial step of endocytosis or transcytosis processes. Afterwards, we propose that the membrane weakens, facilitating changes in cell electrophysiology, including hyperpolarization, and subsequently the influx of Ca^{2+}. The combined effects of US and MBs induces transcytosis of 500 kDa dextran via a dynamin-/caveolae-/clathrin- related pathway. Besides, the acoustically triggered Ca^{2+} influx assists in the transcytosis process partly through PKC pathway, rather than the CAMKII pathway (Scheme1).

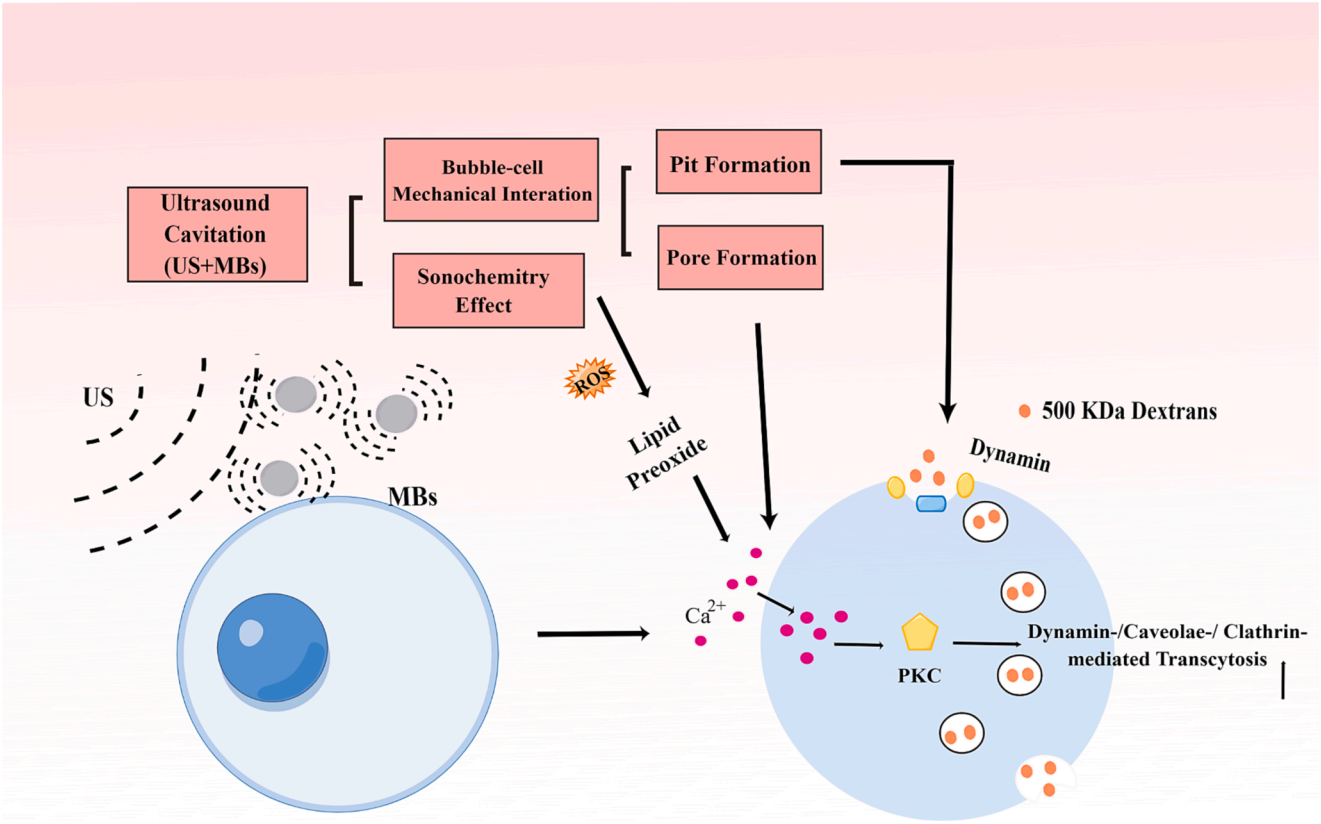

Scheme 1. Cascade of events that lead to an enhanced transport of molecules across the BBB: In Vitro Acoustically-mediated Membrane Deformation Increases Permeability of Macromolecular Substance in Blood-Brain Barrier Opening (BBBO).

5. Conclusion

In this study, we investigated the potential role of mechanical interactions between microbubbles and cells, facilitated by the application of ultrasound in promoting the enhanced extravasation of large molecules across the BBB. Our aim was to provide insights into the mechanisms underlying the increased transcytosis observed during the use of US + MBs. Our results demonstrate that the mechanical interaction between oscillating microbubbles and cell membrane plays a pivotal role in the dynamin-/caveolae-/clathrin- related transcytosis. Additionally, the enhanced transcytosis pathway mediated by US + MBs relies on calcium ion influx in relation with the PKC pathway. Overall, this study provides valuable insights into the potential mechanisms for macromolecular substance permeability across the BBB via acoustic bubble-cell interactions.

CRediT authorship contribution statement

Jifan Chen: Conceptualization, Formal analysis, Investigation, Methodology, Writing – original draft. **Jean-Michel Escoffre:** Data curation, Formal analysis, Methodology, Writing – review & editing. **Oliver Romito:** Formal analysis, Methodology, Writing – original draft. **Tarik Iazourene:** Investigation, Methodology, Writing – original draft. **Antoine Presset:** Methodology, Writing – original draft. **Marie Roy:** Methodology, Writing – original draft. **Marie Potier Cartereau:** Methodology, Writing – original draft. **Christophe Vandier:** Formal analysis, Investigation, Methodology, Writing – original draft. **Yahua Wang:** Investigation, Methodology, Writing – original draft. **Guowei Wang:** Investigation, Methodology, Writing – original draft. **Pintong Huang:** Conceptualization, Funding acquisition, Investigation, Methodology, Supervision, Writing – original draft, Writing – review & editing. **Ayache Bouakaz:** Conceptualization, Formal analysis, Funding acquisition, Investigation, Methodology, Supervision, Validation, Writing – original draft, Writing – review & editing.

Declaration of competing interest

The authors declare that they have no known competing financial interests or personal relationships that could have appeared to influence the work reported in this paper.

Data availability

Data will be made available on request.

Acknowledgements

Funding: This work was supported by National Natural Science Foundation of China (No. 82030048, 82230069) (PH), China Scholarship Council (CSC, No. 202106320283) (JC), China Postdoctoral Science Foundation (No.2023M743114) (JC), Binjiang Institute of Zhejiang Univeristy (NO. ZY202205SMKY001) (PH) as well as from Inserm UMR 1253, iBrain, Université de Tours, Inserm, Tours, France (AB) and PHC Sakura (JME).

Appendix A. Supplementary data

Supplementary data to this article can be found online at https://doi.org/10.1016/j.ultsonch.2024.106768.

References

[1] N.J. Abbott, A.A. Patabendige, D.E. Dolman, S.R. Yusof, D.J. Begley, Structure and function of the blood-brain barrier, Neurobiol. Dis. 37 (2010) 13–25.
[2] B. Obermeier, R. Daneman, R.M. Ransohoff, Development, maintenance and disruption of the blood-brain barrier, Nat. Med. 19 (2013) 1584–1596.
[3] B.J. Andreone, B.W. Chow, A. Tata, B. Lacoste, A. Ben-Zvi, K. Bullock, A.A. Deik, D. D. Ginty, C.B. Clish, C. Gu, Blood-Brain Barrier Permeability Is Regulated by Lipid Transport-Dependent Suppression of Caveolae-Mediated Transcytosis, Neuron 94 (2017) 581–594.e585.
[4] S. Wang, M.E. Karakatsani, C. Fung, T. Sun, C. Acosta, E. Konofagou, Direct brain infusion can be enhanced with focused ultrasound and microbubbles, J. Cereb. Blood Flow Metab. 37 (2017) 706–714.
[5] A.M. Mehta, A.M. Sonabend, J.N. Bruce, Convection-Enhanced Delivery, Neurotherapeutics 14 (2017) 358–371.
[6] D.T. Wiley, P. Webster, A. Gale, M.E. Davis, Transcytosis and brain uptake of transferrin-containing nanoparticles by tuning avidity to transferrin receptor, PNAS 110 (2013) 8662–8667.
[7] G. Morad, C.V. Carman, E.J. Hagedorn, J.R. Perlin, L.I. Zon, N. Mustafaoglu, T. E. Park, D.E. Ingber, C.C. Daisy, M.A. Moses, Tumor-Derived Extracellular Vesicles Breach the Intact Blood-Brain Barrier via Transcytosis, ACS Nano 13 (2019) 13853–13865.
[8] J. Lichota, T. Skjørringe, L.B. Thomsen, T. Moos, Macromolecular drug transport into the brain using targeted therapy, J. Neurochem. 113 (2010) 1–13.
[9] A. Ben-Zvi, B. Lacoste, E. Kur, B.J. Andreone, Y. Mayshar, H. Yan, C. Gu, Mfsd2a is critical for the formation and function of the blood-brain barrier, Nature 509 (2014) 507–511.
[10] C. Zhao, J. Ma, Z. Wang, H. Li, H. Shen, X. Li, G. Chen, Mfsd2a Attenuates Blood-Brain Barrier Disruption After Sub-arachnoid Hemorrhage by Inhibiting Caveolae-Mediated Transcellular Transport in Rats, Transl. Stroke Res. 11 (2020) 1012–1027.
[11] M. Zhou, S.X. Shi, N. Liu, Y. Jiang, M.S. Karim, S.J. Vodovoz, X. Wang, B. Zhang, A. S. Dumont, Caveolae-Mediated Endothelial Transcytosis across the Blood-Brain Barrier in Acute Ischemic Stroke, J. Clin. Med. 10 (2021).
[12] Y. Yang, Q. Li, X. Guo, J. Tu, D. Zhang, Mechanisms underlying sonoporation: Interaction between microbubbles and cells, Ultrason. Sonochem. 67 (2020) 105096.
[13] W.H. Liao, M.Y. Hsiao, Y. Kung, H.L. Liu, J.C. Béra, C. Inserra, W.S. Chen, TRPV4 promotes acoustic wave-mediated BBB opening via Ca(2+)/PKC-δ pathway, J. Adv. Res. 26 (2020) 15–28.
[14] C. Gasca-Salas, B. Fernández-Rodríguez, J.A. Pineda-Pardo, R. Rodríguez-Rojas, I. Obeso, F. Hernández-Fernández, M. Del Álamo, D. Mata, P. Guida, C. Ordás-Bandera, J.I. Montero-Roblas, R. Martínez-Fernández, G. Foffani, I. Rachmilevitch, J.A. Obeso, Blood-brain barrier opening with focused ultrasound in Parkinson's disease dementia, Nat. Commun. 12 (2021) 779.
[15] C.Y. Lin, H.Y. Hsieh, C.M. Chen, S.R. Wu, C.H. Tsai, C.Y. Huang, M.Y. Hua, K. C. Wei, C.K. Yeh, H.L. Liu, Non-invasive, neuron-specific gene therapy by focused ultrasound-induced blood-brain barrier opening in Parkinson's disease mouse model, J. Control. Release 235 (2016) 72–81.
[16] R. Pandit, W.K. Koh, R.K.P. Sullivan, T. Palliyaguru, R.G. Parton, J. Götz, Role for caveolin-mediated transcytosis in facilitating transport of large cargoes into the brain via ultrasound, J. Control. Release 327 (2020) 667–675.
[17] J. Deng, Q. Huang, F. Wang, Y. Liu, Z. Wang, Z. Wang, Q. Zhang, B. Lei, Y. Cheng, The role of caveolin-1 in blood-brain barrier disruption induced by focused ultrasound combined with microbubbles, J. Mol. Neurosci. 46 (2012) 677–687.
[18] A. Zeghimi, J.M. Escoffre, A. Bouakaz, Role of endocytosis in sonoporation-mediated membrane permeabilization and uptake of small molecules: a electron microscopy study, Phys. Biol. 12 (2015) 066007.
[19] B.D. Meijering, L.J. Juffermans, A. van Wamel, R.H. Henning, I.S. Zuhorn, M. Emmer, A.M. Versteilen, W.J. Paulus, W.H. van Gilst, K. Kooiman, N. de Jong, R.J. Musters, L.E. Deelman, O. Kamp, Ultrasound and microbubble-targeted delivery of macromolecules is regulated by induction of endocytosis and pore formation, Circ. Res. 104 (2009) 679–687.
[20] M.S. Karthikesh, X. Yang, The effect of ultrasound cavitation on endothelial cells, Exp. Biol. Med. (Maywood) 246 (2021) 758–770.
[21] K. Kooiman, A.F. van der Steen, N. de Jong, Role of intracellular calcium and reactive oxygen species in microbubble-mediated alterations of endothelial layer permeability, IEEE Trans. Ultrason. Ferroelectr. Freq. Control 60 (2013) 1811–1815.
[22] J.M. Escoffre, P. Campomanes, M. Tarek, A. Bouakaz, New insights on the role of ROS in the mechanisms of sonoporation-mediated gene delivery, Ultrason. Sonochem. 64 (2020) 104998.
[23] T.A. Tran, J.Y. Le Guennec, P. Bougnoux, F. Tranquart, A. Bouakaz, Characterization of cell membrane response to ultrasound activated microbubbles, IEEE Trans. Ultrason. Ferroelectr. Freq. Control 55 (2008) 43–49.
[24] V. Coelho-Santos, R. Socodato, C. Portugal, R.A. Leitão, M. Rito, M. Barbosa, P. O. Couraud, I.A. Romero, B. Weksler, R.D. Minshall, C. Fontes-Ribeiro, T. Summavielle, J.B. Relvas, A.P. Silva, Methylphenidate-triggered ROS generation promotes caveolae-mediated transcytosis via Rac1 signaling and c-Src-dependent caveolin-1 phosphorylation in human brain endothelial cells, Cell. Mol. Life Sci. 73 (2016) 4701–4716.
[25] Y. Song, J. Chen, C. Zhang, L. Xin, Q. Li, Y. Liu, C. Zhang, S. Li, P. Huang, Mechanosensitive Channel Piezo1 Induces Cell Apoptosis in Pancreatic Cancer by Ultrasound with Microbubbles. 25 (iScience 2022,) 103733.
[26] K.R. Kalari, K.J. Thompson, A.A. Nair, X. Tang, M.A. Bockol, N. Jhawar, S. K. Swaminathan, V.J. Lowe, K.K. Kandimalla, BBBomics-Human Blood Brain Barrier Transcriptomics Hub, Front. Neurosci. 10 (2016) 71.
[27] M.A. Lopez-Ramirez, D.K. Male, C. Wang, B. Sharrack, D. Wu, I.A. Romero, Cytokine-induced changes in the gene expression profile of a human cerebral microvascular endothelial cell-line, hCMEC/D3, Fluids Barriers CNS 10 (2013) 27.
[28] M.S. Schappe, K. Szteyn, M.E. Stremska, S.K. Mendu, T.K. Downs, P.V. Seegren, M. A. Mahoney, S. Dixit, J.K. Krupa, E.J. Stipes, J.S. Rogers, S.E. Adamson,

N. Leitinger, B.N. Desai, Chanzyme TRPM7 Mediates the Ca(2+) Influx Essential for Lipopolysaccharide-Induced Toll-Like Receptor 4 Endocytosis and Macrophage Activation, Immunity 48 (2018) 59–74.e55.
[29] M. Kreft, M. Potokar, M. Stenovec, T. Pangrsic, R. Zorec, Regulated exocytosis and vesicle trafficking in astrocytes, Ann. N. Y. Acad. Sci. 1152 (2009) 30–42.
[30] P. Stokłosa, S. Kappel, C. Peinelt, A Novel Role of the TRPM4 Ion Channel in Exocytosis, Cells 11 (2022) 1793.
[31] Y. Zheng, J. Wu, W. Shan, L. Wu, R. Zhou, M. Liu, Y. Cui, M. Zhou, Z. Zhang, Y. Huang, Multifunctional Nanoparticles Enable Efficient Oral Delivery of Biomacromolecules via Improving Payload Stability and Regulating the Transcytosis Pathway, ACS Appl. Mater. Interfaces 10 (2018) 34039–34049.
[32] S. Ayloo, C. Gu, Transcytosis at the blood–brain barrier, Curr. Opin. Neurobiol. 57 (2019) 32–38.
[33] M.N. Bao, L.J. Zhang, B. Tang, D.D. Fu, J. Li, L. Du, Y.N. Hou, Z.L. Zhang, H. W. Tang, D.W. Pang, Influenza A Viruses Enter Host Cells via Extracellular Ca(2+) Influx-Involved Clathrin-Mediated Endocytosis, ACS Appl Bio Mater 4 (2021) 2044–2051.
[34] B.S. Joshi, I.S. Zuhorn, Heparan sulfate proteoglycan-mediated dynamin-dependent transport of neural stem cell exosomes in an in vitro blood-brain barrier model, Eur. J. Neurosci. 53 (2021) 706–719.
[35] P.M. Azizi, R.E. Zyla, S. Guan, C. Wang, J. Liu, S.S. Bolz, B. Heit, A. Klip, W.L. Lee, Clathrin-dependent entry and vesicle-mediated exocytosis define insulin transcytosis across microvascular endothelial cells, Mol. Biol. Cell 26 (2015) 740–750.